Biochimica et Biophysica Acta 1817 (2012) 1925–1936

Contents lists available at SciVerse ScienceDirect

Biochimica et Biophysica Acta

journal homepage: www.elsevier.com/locate/bbabio

Metabolic consequences of *NDUFS4* gene deletion in immortalized mouse embryonic fibroblasts ☆

Federica Valsecchi [a,b], Claire Monge [c], Marleen Forkink [a], Ad J.C. de Groof [c], Giovanni Benard [d], Rodrigue Rossignol [d], Herman G. Swarts [a], Sjenet E. van Emst-de Vries [a], Richard J. Rodenburg [b], Maria A. Calvaruso [b], Leo G.J. Nijtmans [b], Bavo Heeman [a], Peggy Roestenberg [a], Be Wieringa [c], Jan A.M. Smeitink [b], Werner J.H. Koopman [a,*], Peter H.G.M. Willems [a]

[a] Department of Biochemistry, Nijmegen Centre for Molecular Life Sciences, Radboud University Nijmegen Medical Centre, Nijmegen, The Netherlands
[b] Department of Pediatrics, Nijmegen Centre of Mitochondrial Disorders, Radboud University Nijmegen Medical Centre, Nijmegen, The Netherlands
[c] Department of Cell Biology, Nijmegen Centre for Molecular Life Sciences, Radboud University Nijmegen Medical Centre, Nijmegen, The Netherlands
[d] Institut National de la Santé et de la Recherche Médicale (INSERM), Universite Victor Segalen-Bordeaux 2, EA4576 Maladies Rares: Génétique et Métabolisme, Bordeaux, France

ARTICLE INFO

Article history:
Received 31 January 2012
Received in revised form 1 March 2012
Accepted 4 March 2012
Available online 11 March 2012

Keywords:
Metabolic disorder
Oxidative phosphorylation
Respirometry
Live-cell microscopy
Glycolysis

ABSTRACT

Human mitochondrial complex I (CI) deficiency is associated with progressive neurological disorders. To better understand the CI pathomechanism, we here studied how deletion of the CI gene *NDUFS4* affects cell metabolism. To this end we compared immortalized mouse embryonic fibroblasts (MEFs) derived from wildtype (wt) and whole-body *NDUFS4* knockout (KO) mice. Mitochondria from KO cells lacked the NDUFS4 protein and mitoplasts displayed virtually no CI activity, moderately reduced CII, CIII and CIV activities and normal citrate synthase and CV (F_oF_1-ATPase) activity. Native electrophoresis of KO cell mitochondrial fractions revealed two distinct CI subcomplexes of ~830 kDa (enzymatically inactive) and ~200 kDa (active). The level of fully-assembled CII–CV was not affected by *NDUFS4* gene deletion. KO cells exhibited a moderately reduced maximal and routine O_2 consumption, which was fully inhibited by acute application of the CI inhibitor rotenone. The aberrant CI assembly and reduced O_2 consumption in KO cells were fully normalized by *NDUFS4* gene complementation. Cellular [NAD^+]/[NADH] ratio, lactate production and mitochondrial tetramethyl rhodamine methyl ester (TMRM) accumulation were slightly increased in KO cells. In contrast, *NDUFS4* gene deletion did not detectably alter [$NADP^+$]/[NADPH] ratio, cellular glucose consumption, the protein levels of hexokinases (I and II) and phosphorylated pyruvate dehydrogenase (P-PDH), total cellular adenosine triphosphate (ATP) level, free cytosolic [ATP], cell growth rate, and reactive oxygen species (ROS) levels. We conclude that the NDUFS4 subunit is of key importance in CI stabilization and that, due to the metabolic properties of the immortalized MEFs, *NDUFS4* gene deletion has only modest effects at the live cell level. This article is part of a special issue entitled: 17th European Bioenergetics Conference (EBEC 2012).

1. Introduction

Mitochondria generate energy in the form of adenosine triphosphate (ATP) and play a crucial role in cell metabolism, signal transduction and survival. Structurally, mitochondria consist of an outer membrane (MOM) that envelops a highly folded inner membrane (MIM). The latter surrounds the mitochondrial matrix compartment where many metabolic reactions take place [1]. Proper mitochondrial functioning requires the presence of a sufficiently large proton gradient across the MIM. This gradient is maintained by the action of the electron transport chain (ETC), which consists of 4 multi-subunit complexes [2]. The first complex (CI) extracts electrons from reduced nicotinamide adenin-dinucleotide (NADH) and donates them to coenzyme Q (CoQ or ubiquinone), allowing their transport to complex III (CIII). Also complex II (CII) donates electrons to CoQ by liberating them from succinate. Next, electrons are transported by cytochrome-*c* (cyt-*c*) to complex IV (CIV) where they are donated to molecular oxygen (O_2) to form water (H_2O). At CI, CIII and CIV the energy released by the electron transport is used to

Abbreviations: ROS, reactive oxygen species; CI, complex I or NADH:ubiquinone oxidoreductase; $\Delta\psi$, mitochondrial membrane potential; ETC, electron transport chain; MIM, mitochondrial inner membrane; MOM, mitochondrial outer membrane; OXPHOS, oxidative phosphorylation; PMF, proton-motive force; ROS, reactive oxygen species; TMRM, tetramethyl rhodamine methyl ester

☆ This article is part of a special issue entitled: 17th European Bioenergetics Conference (EBEC 2012).

* Corresponding author at: 286 Biochemistry, Nijmegen Centre for Molecular Life Sciences, Radboud University Nijmegen Medical Centre, P.O. Box 9101, NL-6500 HB Nijmegen, The Netherlands. Tel.: +31 24 3614589; fax: +31 24 3616413.
E-mail address: w.koopman@ncmls.ru.nl (W.J.H. Koopman).

0005-2728/$ – see front matter © 2012 Elsevier B.V. All rights reserved.
doi:10.1016/j.bbabio.2012.03.006

expel protons from the mitochondrial matrix across the MIM. The latter generates an inwardly directed trans-MIM electrochemical proton motive force (PMF), associated with an inside-negative mitochondrial membrane potential ($\Delta\psi$), and a chemical proton gradient (ΔpH). The PMF-driven backflow of protons is used by the F_oF_1-ATPase (CV) to drive mitochondrial ATP synthesis. Together, the ETC and CV constitute the oxidative phosphorylation (OXPHOS) system [3].

Mitochondrial CI (or NADH:ubiquinone oxidoreductase; EC 1.6.5.3) consists of 45 different subunits and constitutes the largest OXPHOS complex with a molecular weight of ~1000 kDa [2,4–7]. Seven of the CI subunits are encoded by the mitochondrial DNA (mtDNA) and the remainder by nuclear DNA (nDNA). The CI catalytic core consists of 14 evolutionary conserved "structural" subunits that, in humans, are encoded by 7 nDNA (*NDUFV1*, *NDUFV2*, *NDUFS1*, *NDUFS2*, *NDUFS3*, *NDUFS7*, *NDUFS8*) and the 7 mtDNA genes (*ND1–ND6* and *ND4L;* [2,8]). The remainder of CI consists of 31 nDNA-encoded supernumerary ("accessory") subunits, of which it is presumed that they do not directly participate in the catalytic action of CI [2,9]. In vitro and live-cell experiments suggest that biogenesis of CI involves the stepwise assembly of pre-assembled modules [5,10–13]. This process is assisted by at least 4 assembly-factors (NDUFAF1–NDUFAF4), CIII and CIV [2,6,7,14]. In humans, mutations in mtDNA- and nDNA-encoded CI structural, assembly-factor and accessory genes are associated with isolated CI deficiency (OMIM 252010). Currently, such mutations have been described for all 7 mitochondrial mtDNA-encoded genes, all 4 known assembly factors and 17 of the nDNA-encoded genes [2,7,15]. Mutations in nDNA-encoded CI subunits are generally inherited in an autosomal recessive manner and induce CI deficiency, which is associated with a range of progressive neurological disorders, often characterized by an early onset and short devastating course [16].

The *NDUFS4* gene is one of the genes often mutated in isolated human CI deficiency [17–24]. *NDUFS4* mutations are generally associated with Leigh syndrome (OMIM 256000), which is an early-onset progressive neurodegenerative disorder with a characteristic neuropathology. The latter consists of focal, bilateral lesions in one or more areas of the central nervous system, including the brainstem, thalamus, basal ganglia, cerebellum, and spinal cord [16]. The *NDUFS4* gene encodes the NDUFS4 subunit of CI (a.k.a. the "AQDQ" subunit), an 18-kDa protein. Evidence has been provided that this protein can be C-terminally phosphorylated by protein kinase A (PKA) in a cAMP-dependent manner [23,24]. This phosphorylation appears to be involved in mitochondrial import and maturation of the NDUFS4 protein, exchange of damaged against native NDUFS4 protein in intact CI and regulation of CI activity.

Future drug testing and (mitigative) treatment requires a proper understanding of the clinical pathomechanism of CI deficiency. To this end, suited cell and animal models need to be developed and experimentally characterized. Recently, the first whole-body knock-out (KO) mouse model for isolated CI deficiency was presented [25]. To create these KO animals, exon 2 of the *NDUFS4* gene was deleted (NDUFS4$^{-/-}$ mice). This exon encodes the last part of the mitochondrial targeting sequence (MTS) and the first 17 amino acids of the NDUFS4 protein. Excision of exon 2 produces a frameshift precluding the synthesis of mature NDUFS4. Similar to human patients, KO animals displayed encephalomyopathy, retarded grow rate, lethargy, loss of motor skills, blindness and a high lactate level [25]. Here we studied the cell metabolic consequences of *NDUFS4* gene deletion by comparing immortalized mouse embryonic fibroblasts (MEFs) from wildtype (wt) and *NDUFS4*$^{-/-}$ mice. It was found that MEFs from *NDUFS4* knockout animals contain an active but destabilized complex I and that *NDUFS4* gene deletion triggers a slightly more glycolytic cellular phenotype. Interestingly, *NDUFS4* gene deletion was not associated with increased ROS levels or detectable alterations in total and free cytosolic ATP levels. In the light of these observations, we discuss the suitability of immortalized cell systems and/or high-glucose culture conditions to study the (patho)physiology of mitochondrial (dys)function.

2. Materials and methods

2.1. Generation and culturing of immortalized mouse embryonic fibroblasts

Primary mouse embryonic fibroblast (MEF) cultures were generated from individual E12.5–13.5 embryos isolated from the intercross of heterozygous *NDUFS4*$^{+/-}$ mice [25]. In brief, embryos were dissected and the head and the internal organs were removed. The remaining tissue was minced and digested for 15 min with Trypsin-EDTA. This procedure was repeated until the tissue was completely in suspension. The suspension was seeded in a T75 flask with DMEM medium (no. 10938, Invitrogen, Breda, The Netherlands), containing 25 mM D-glucose and supplemented with L-glutamine (4 mM final concentration), 1 mM sodium pyruvate, 10% (v/v) Fetal Calf Serum (FCS, Greiner Bio-one, Frickenhausen, Germany) and 0.1% (v/v) Gentamycin (Invitrogen). The obtained cells were cultured in a humidified atmosphere of 95% air and 5% CO_2 at 37 °C, expanded for two passages and genotyped using polymerase chain reaction (PCR) analysis and specific forward and reverse primers designed for the *NDUFS4* gene: 5′-AGCCTGTTCTCATACCTCGG-3′ (forward; ~1229 bp) and 5′-TTGTGCTTACAGGTTCAAAGTGA-3′ (reverse;~429 bp). DNA was isolated from MEFs using the easy-DNA™ kit (Invitrogen), according to the manufacturer's instructions. The PCR was performed using a Phire hot start II DNA Polymerase kit (Finnzymes, Espoo, Finland). The samples were heated at 98 °C (40 s). Subsequent annealing and extension were carried out at 52 °C (10 s) and at 72 °C (1 min), respectively. Next, 34 cycles were carried out at 98 °C (10 s). Final extension was performed at 72 °C (10 min) on a Peltier Thermal Cycler (MJ Research PTC-200). Using the above strategy, primary MEF cell lines were generated from two different wt (wt1, wt2) and two different knock-out (KO) animals (KO1, KO2). Primary cultures were spontaneously immortalized using the 3T3 protocol [26] and grown in the above DMEM medium.

2.2. Retroviral complementation of immortalized mouse embryonic fibroblasts

The cDNA for the NDUFS4 subunit of CI was obtained by PCR of reverse-transcribed mRNA using oligonucleotide primer sequences taken from public databases and Pfu Turbo DNA polymerase (Agilent Technologies-Stratagene, Amstelveen, The Netherlands). Subsequently, the cDNA was subcloned in bacterial cloning vectors and verified by DNA sequencing. The cDNA was used as template DNA for a second round of PCR, in which appropriate restriction sites and a 5′ Kozak sequence (GCCACCATG) were introduced by addition of the respective DNA sequences to the primers. Subsequently, the cDNA, prepared with a Kozak sequence via the PCR primer, was cloned into retroviral expression vector pLZRS-ires-Zeo. For production of helper-free recombinant retrovirus, amphotrophic Phoenix ΦNX-A packaging cells [27–29] were grown in DMEM and transfected with the pLZRS-hNDUFS4-ires-Zeo plasmid using Lipofectamine 2000 (Invitrogen). Viral supernatants (3 ml) supplemented with polybrene were added to *NDUFS4* KO MEFs (see above), seeded one day prior to infection at a density of 100,000/well in 6-well culture plates, and infection was allowed for 24 h. Afterward, medium was replaced by a selection medium with Zeocin (Invitrogen), for 14 days. Using the above procedure, complemented stable cell lines were generated from wt1, KO1 and KO2 cells in which the *NDUFS4*–cDNA was retrovirally introduced (wt1 + S4, KO1 + S4, KO2 + S4). Similarly, additional control cell lines were generated by retrovirally transfecting wt and KO MEFs with an "empty" virus (wt1 + e, KO1 + e and KO2 + e).

2.3. Culture of human skin fibroblasts

Human skin fibroblasts of a healthy individual (CT5120) and two patients with isolated CI deficiency due to a mutation in the *NDUFS4* gene (VPEEKH167/VEKSIstop: P5737 and R106X: P5260; [16]) were cultured in HEPES-buffered (25 mM) medium 199 (M199; Invitrogen) with Earle's salt, containing 5.5 mM D-glucose and 0.7 mM L-glutamine, in a humidified atmosphere of 95% air and 5% CO_2 at 37 °C. M199 was supplemented with 10% (v/v) fetal calf serum, 100 IU/ml penicillin and 100 IU/ml streptomycin (Invitrogen). The patient cells were obtained from children in whom an isolated deficiency (OMIM 252010) was confirmed in both muscle tissue and cultured skin fibroblasts. Biopsies were performed following informed parental consent and according to the relevant Institutional Review Boards.

2.4. Enzyme activity measurement

Activity of mitochondrial enzymes was determined in isolated mitoplasts (i.e. isolated mitochondria without their outer membranes) as described previously [30].

2.5. Native gel electrophoresis

MEFs were harvested by trypsinization, washed twice with ice-cold PBS and resuspended in ice-cold PBS (100 μl). To obtain a mitochondria-enriched fraction, cells were incubated with 4 mg/ml digitonin (Sigma-Aldrich, St. Louis, MO, USA) in a final volume of 200 μl for 10 min on ice. Next, the cells were centrifuged (10 min, 10,000 *g*, 4 °C) and mitochondrial pellets were washed twice with 1 ml ice-cold PBS and stored overnight (−20°C). Pellets were solubilized in 100 μl "ACBT buffer" containing 1.5 M aminocaproic acid (Sigma) and 75 mM Bis-Tris (Sigma). To isolate mitochondrial OXPHOS complexes 20 μl 10% (w/v) β-lauryl maltoside (Sigma) was added and the solution was incubated for 10 min on ice. Following centrifugation (30 min, 10,000 *g*, 4 °C), the protein concentration was determined using a protein assay kit (Biorad laboratories, Hercules, USA). For quantitative analysis the gels were loaded with exactly 20 μg of mitochondrial protein. BN-PAGE was performed using a native page TM 4–16% Bis-Tris Gel (Invitrogen). Blotting was performed using an iBlot Gel Transfer Stacks PVDF with iBlot system (Invitrogen). Immunodetection was carried out by incubating the blots with antibodies directed against the NDUFA9 subunit of CI (CI-39; Mitosciences, Eugene, Oregon), the 70 kDa subunit of CII (CII-70, Invitrogen), the core2 subunit of CIII (CIII-core2; Mitosciences), subunit 2 of CIV (CIV-2; Mitosciences) and the α subunit of CV (CV-α; Mitosciences). The secondary antibody consisted of IRDye 800CW Conjugated Goat Anti-mouse IgG (H + L), Highly Cross Adsorbed (Li-Cor, Lincoln, USA), diluted 1:10,000. Fluorescence scanning was performed using an Odyssey Imaging system (Li-Cor) and fluorograms were inverted for visualization purposes. For in-gel activity analysis the gel was incubated overnight with 2 mM Tris/HCl, 0.1 mg/ml NADH, 2.5 mg/ml nitro blue tetrazolium (NBT; Sigma) at 4 °C and scanned.

2.6. SDS-PAGE analysis of NDUFS4 protein levels

For human skin fibroblasts and MEFs, mitochondria were isolated as described in the previous section. In case of mouse muscle, mitochondria-enriched fractions were obtained as described previously [31]. SDS-PAGE was performed with 5–20% gradient gel using 20 μg of protein for each lane. Proteins were electrophoretically transferred to a PVDF membrane (Millipore, Amsterdam, The Netherlands) using a transfer buffer containing 20% (v/v) methanol, 25 mM Tris–HCl, 192 mM glycine and 0.02% (w/v) SDS. After blotting, membranes were blocked for 1 h in Odyssey blocking buffer (Li-Cor) and PBS (ratio 1:1). Next, the blots were incubated with an anti-NDUFS4 monoclonal antibody (MS104, Mitosciences) for 4 h. Subsequently, the blots were washed 3 times with 0.1% (w/v) Tween 20 containing PBS (PBS-Tween) followed by incubation with the secondary antibody (IRDye 800CW Conjugated Goat Anti-mouse IgG (H + L), Highly Cross Adsorbed; diluted 1:10,000; Li-Cor). Fluorescence scanning was performed using an Odyssey Imaging system (Li-Cor) and fluorograms were inverted for visualization purposes.

2.7. SDS-PAGE analysis of glycolytic enzyme levels

Cells were grown in T175 flasks, washed twice with PBS and scraped off in 2 ml of cold isolation buffer (225 mM mannitol, 10 mM HEPES, 75 mM sucrose, 0.1 mM EGTA, pH 7.4, 1×) protease inhibitor cocktail (Roche Diagnostics GmbH, Mannheim, Germany). Cells were collected and centrifuged (10 min, 2000 *g*, 4 °C). The resulting pellet was resuspended in cold isolation buffer and homogenized on ice with a 2 ml glass homogenizer. Subsequently the homogenate was centrifuged (5 min, 1000 *g*, 4 °C), the pellet was discarded and the obtained supernatant was centrifuged (15 min, 15,000 *g*, 4 °C). The resulting supernatant and pellet were used as cytosolic and mitochondrial fractions, respectively. The mitochondrial fraction was then washed twice with cold washing buffer (395 mM sucrose, 10 mM HEPES, 0.1 mM EGTA at pH 7.4) and centrifuged (15 min, 15,000 *g*, 4 °C). Finally, the obtained pellet was resuspended in 500 μl of washing buffer, frozen in liquid nitrogen and stored at −80 °C. Exactly 25 μg of protein was loaded on a 10% SDS-PAGE gel. Next, protein was transferred electrophoretically to a PVDF membrane (Millipore) in transfer buffer. After blotting membranes were blocked for 1 h with 5% (w/v) non-fat dried milk in 0.1% (w/v) Tween 20 containing PBS (PBS-Tween). Afterward the blots were rinsed twice with PBS-Tween and incubated over night at 4 °C with polyclonal primary antibodies directed against HK-I (sc-6521, Santa Cruz Biotech. Inc., Santa Cruz, USA), HK-II (sc-6519, Santa Cruz), P-PDH pSer293 (Calbiochem, San Diego, USA), β-tubulin (E7, Developmental Studies Hybridoma Bank, University of Iowa, Iowa City, Iowa) or VDAC (the mitochondrial voltage dependent anion channel; a.k.a. porin; Calbiochem, San Diego, USA). Subsequently, blots were washed 3 times with PBS and incubated with secondary antibodies anti-goat for HK-I and II and anti-rabbit for P-PDH. Fluorescence was quantified using the Odyssey Imaging system described above (Li-Cor).

2.8. Quantification of routine oxygen consumption in intact cells

Cells were grown in DMEM containing 25 mM glucose and 4 mM glutamine [32]. Routine (endogenous) respiration was measured using 2 million cells in this DMEM medium, as described previously [33] by monitoring oxygen consumption at 37 °C in a 1 ml, thermostatically controlled, chamber equipped with a Clark oxygen electrode (Oxy 1, Hansatech, Pentney, UK).

2.9. Quantification of routine, leak and maximal oxygen consumption in intact cells

DMEM culture medium was collected and 1 million cells were trypsinized, washed and resuspended in 60 μl of the collected culture medium. Part of this suspension (50 μl) was used for cellular O_2 consumption analysis. O_2 consumption was measured at 37 °C using polarographic oxygen sensors in a two-chamber Oxygraph (OROBOROS Instruments, Innsbruck, Austria) using an established protocol [34].

2.10. Quantification of cellular NAD^+, NADH, $NADP^+$ and NADPH levels

Determination of NAD^+, NADH, $NADP^+$ and NADPH levels was performed in whole cell homogenates as described previously [35].

2.11. Quantification of cell number, extracellular glucose concentration and extracellular lactate concentration

Cells were seeded in 96-well plates and cell numbers were determined using Sulforhodamine B staining (SRB; Sigma). To this end, cells were fixed after 24, 48 and 72 h using trichloroacetic acid (TCA) and 50 μl of 0.5% (v/v) SRB solution was added to each well. After 30 min of incubation at room temperature the SRB solution was removed and the cells were washed with acetic acid 1% (v/v) and further incubated for 3 h at 60 °C to fully evaporate the acetic acid. Next, 150 μl of 10 mM Tris was added to each well and absorbance was measured at 510 nm in a plate reader (Benchmark Plus, Bio-rad). Glucose levels were determined by harvesting the culture medium at 72 h and using the Amplex Red glucose/glucose oxidase assay kit (Invitrogen). Lactate levels were determined by harvesting the culture medium following 72 h of culturing and using the Amplex Red glucose/glucose oxidase kit (Invitrogen) in which lactate oxidase was used instead of glucose oxidase.

2.12. Quantification of mitochondrial NAD(P)H autofluorescence

MEFs were grown on glass coverslips (24 mm) to 70% confluence. Prior to imaging, the medium was replaced by a HEPES-Tris (HT) solution containing 5.5 mM D-glucose (132 mM NaCl, 4.2 mM KCl, 1 mM $CaCl_2$, 1 mM $MgCl_2$, and 10 mM HEPES (pH 7.4)). For fluorescence measurements, dishes were mounted in a thermostatic (37 °C) superfusion chamber placed on the stage of an inverted microscope (Axiovert 200 M; Carl Zeiss, Jena, Germany) equipped with a ×40, 1.3 NA F Fluar objective. NAD(P)H autofluorescence was detected using 360 nm excitation light delivered by a monochromator (Polychrome IV; TILL Photonics, Gräfelfing, Germany). Fluorescence light was directed by a 430DCLP dichroic mirror (Omega Optical Inc., Brattleboro, USA) through a 510WB40 emission filter (Omega) onto a CoolSNAP HQ monochrome CCD-camera (Roper Scientific, Ottobrunn, Germany). The integration time of the CCD camera was set at 1 s and hardware was controlled with Metafluor 6.0 software (MDS Analytical Technologies, Molecular Devices, Sunnyvale, USA). The mean mitochondrial fluorescence intensity was determined by placing a region of interest (ROI) in a mitochondria-dense region of the cell. The intensity for this ROI was background corrected using a nearby extracellular ROI [36,37].

2.13. Quantification of total cellular ATP levels

ATP content was measured in lysed cells using the bioluminescent ATP kit HS II (Roche Applied Science, Almere, The Netherlands). Cells grown in DMEM medium for 6 days were washed with PBS, detached with trypsin and resuspended in fresh DMEM (100 μl of a cell suspension containing 2 million cells/ml). Subsequently cells were lysed to release the intracellular ATP using the lysis buffer included in the kit. 100 μl of the lysate was analyzed in a 96 well plate luminometer (Luminoskan, Thermo Fisher Scientific, Breda, The Netherlands) using the luciferine–luciferase reaction system provided in the kit. 100 μl of luciferine/ase was injected in the wells and after 10 s of incubation the bioluminescent signal was quantified using an integration time of 1 s. Quantification was performed by generating a standard curve using ATP provided in the kit.

2.14. Quantification of free cytosolic ATP levels

To visualize free cytosolic ATP levels, the fluorescence resonance energy transfer (FRET)-based reporter protein ('ATeam' 1.03) was used. This sensor was composed of the ε subunit of the bacterial F_oF_1-ATP synthase sandwiched between cyan-and yellow-fluorescent protein variants [38,39]. ATeam was expressed in the cells using baculoviral transduction. To this end, a Bac-to-Bac system normally used for protein production in *Spodoptera frugiperda* insect cells (Sf9) was made suitable for protein expression in mammalian cells by cloning the vesicular stomatitis virus G protein cDNA behind the P10 promoter of the pFastBacDual vector. Next, the CMV promoter and Gateway (Invitrogen) destination elements (i.e. a cassette containing the chloramphenicol resistance gene and the ccdB gene flanked by attR1 and attR2 sites) were introduced in the pFastBacDual vector [40]. The SpeI/HindIII fragment of human pcDNA3-ATeam-cyto was ligated into the SpeI/HindIII sites of the pFastBacDual vector. Baculoviruses were produced as described in the Bac-to-Bac manual (Invitrogen). To express ATeam, cells were seeded on a WillCo-Dish (22 mm; Intracel Ltd., Royston, UK) and cultured for 24 h. Cells were then infected with the ATeam baculovirus (6% v/v) in HBSS buffer (Hank's Balanced Salt Solution 1×, Invitrogen) containing 0.25% v/v of sodium butyrate (Sigma) and cultured for 6 h. Afterward the buffer was removed and the cells were incubated with complete DMEM medium for another 24 h. For fluorescence measurements, dishes were mounted in a thermostatic (37 °C) superfusion chamber placed on the stage of an inverted microscope (Axiovert 200 M; Carl Zeiss) equipped with a ×40, 1.3 NA F Fluar objective. During measurements cells were maintained in HT medium. ATeam was excited at 435 nm using a monochromator (TILL Photonics) and fluorescence emission light was directed by a 455DRLP dichroic mirror through either a 480AF30 (CFP-signal) or a 535AF26 emission filter (YFP-signal) (Omega Optical Inc.) onto a CoolSNAP HQ monochrome CCD-camera (Roper Scientific). The integration time of the CCD camera was set at 200 ms and hardware was controlled with Metafluor 6.0 software (MDS Analytical Technologies). Steady-state analysis was performed by randomly measuring 10 fields of cells and calculating the ratio between the background-corrected YFP and CPF fluorescence signal for a cytosolic region of interest (ROI) in each individual cell. Similarly, ATeam time-lapse analysis was carried out by acquiring YFP and CFP images at an interval of 6 s. In the latter experiments a superfusion system was used to replace the glucose-containing HT medium by a HT medium in which the glucose was replaced by an equimolar amount of the glycolysis inhibitor 2-deoxy-D-glucose (2-DG; Sigma).

2.15. Quantification of mitochondrial TMRM accumulation

Microscopy images of cells stained with 10 nM TMRM (tetramethyl rhodamine methyl ester; Invitrogen) were acquired using the above microscopy system as described in detail before [41]. During measurements cells were maintained in HT medium. The mean mitochondrial fluorescence intensity was determined by drawing an ROI in a mitochondria-dense perinuclear region of the cells. The intensity for this ROI was background corrected using a nearby extracellular ROI of identical size. Similarly, the background-corrected nuclear TMRM intensity was determined using an ROI placed in the nucleus [2].

2.16. Quantification of reactive oxygen species levels

MEFs were grown on glass coverslips (24 mm) to 70% confluence and incubated in DMEM medium containing 10 μM hydroethidine (HEt; Invitrogen) for exactly 10 min at 37 °C. HEt readily enters the cell and can be oxidized to form two fluorescent products: ethidium (Et^+) and 2-hydroxyethidium (2-OH-Et^+). The reaction was stopped by thoroughly washing the cells with PBS to remove excess HEt followed by placing the cells in HT solution. Fluorescence images were collected using the microscope system described above. During measurements cells were maintained in HT medium. HEt oxidation products were visualized using a 490 nm excitation wavelength, a 525DRLP dichroic mirror (Omega) and a 565 ALP emission filter (Omega). Routinely, 10 fields of view were analyzed per coverslip using an acquisition time of 100 ms. The mean mitochondrial

fluorescence intensity was determined by drawing an ROI in a mitochondria-dense perinuclear region of the cells. The intensity for this ROI was background corrected using a nearby extracellular ROI.

2.17. Image processing and data analysis

Image processing and analysis were performed using Metamorph 6.0 (MDS Analytical Technologies) and Image Pro Plus 6.1 software (Media Cybernetics, Inc., Bethesda, MD, USA). Visualization of numerical results, curve fitting and statistical analysis was performed using Origin Pro 6.1 software (OriginLab Corp., Northampton, MA, USA). Unless stated otherwise, average data is presented as the mean ± SEM (standard error of the mean). Statistical differences were determined using either a two-population or one-population Student's *t*-test (Bonferroni corrected).

3. Results

3.1. Mitochondria-enriched fractions from KO cells do not contain detectable amounts of NDUFS4 protein

Immortalized mouse embryonic fibroblast (MEF) cell lines were generated from two wildtype (wt) mouse embryos (wt1, wt2) and two *NDUFS4* KO mouse embryos (KO1, KO2). Genotyping confirmed that the 800 bp fragment (corresponding to *NDUFS4* gene) was absent in the KO cell lines (Fig. 1A). SDS-PAGE analysis of mitochondria-enriched cell fractions demonstrated that NDUFS4 protein was absent in MEFs and muscle cells of the KO animal (Fig. 1B; left and middle panels). Similar results were obtained in fibroblasts from patients with CI deficiency carrying an *NDUFS4* mutation (Fig. 1B; right panel; P5737, P5260). Reintroduction of the *NDUFS4* gene in the KO cells led to reappearance of the NDUFS4 protein (Fig. 1B; left panel; "KO1 + S4").

3.2. NDUFS4 gene deletion reduces the maximal activity of CI, CII, CIII and CIV but does not affect this parameter for CV and citrate synthase in mitoplasts

Analysis of OXPHOS complex activity in mitoplasts under V_{max} conditions revealed that citrate synthase (CS) activity was not affected in KO cells (Fig. 1C), whereas CI activity was virtually undetectable (Fig. 1D). *NDUFS4* gene deletion also reduced the average maximal activity of CII (by 18%; Fig. 1E), CIII (by 23%; Fig. 1F), combined CII + CIII ("SCC", by 44%; Fig. 1G) and CIV (by 25%; Fig. 1H). In contrast, the average CV activity was not affected (Fig. 1I). These results demonstrate that *NDUFS4* gene deletion greatly reduces maximal CI activity and also lowers the activities of CII, CIII and CIV.

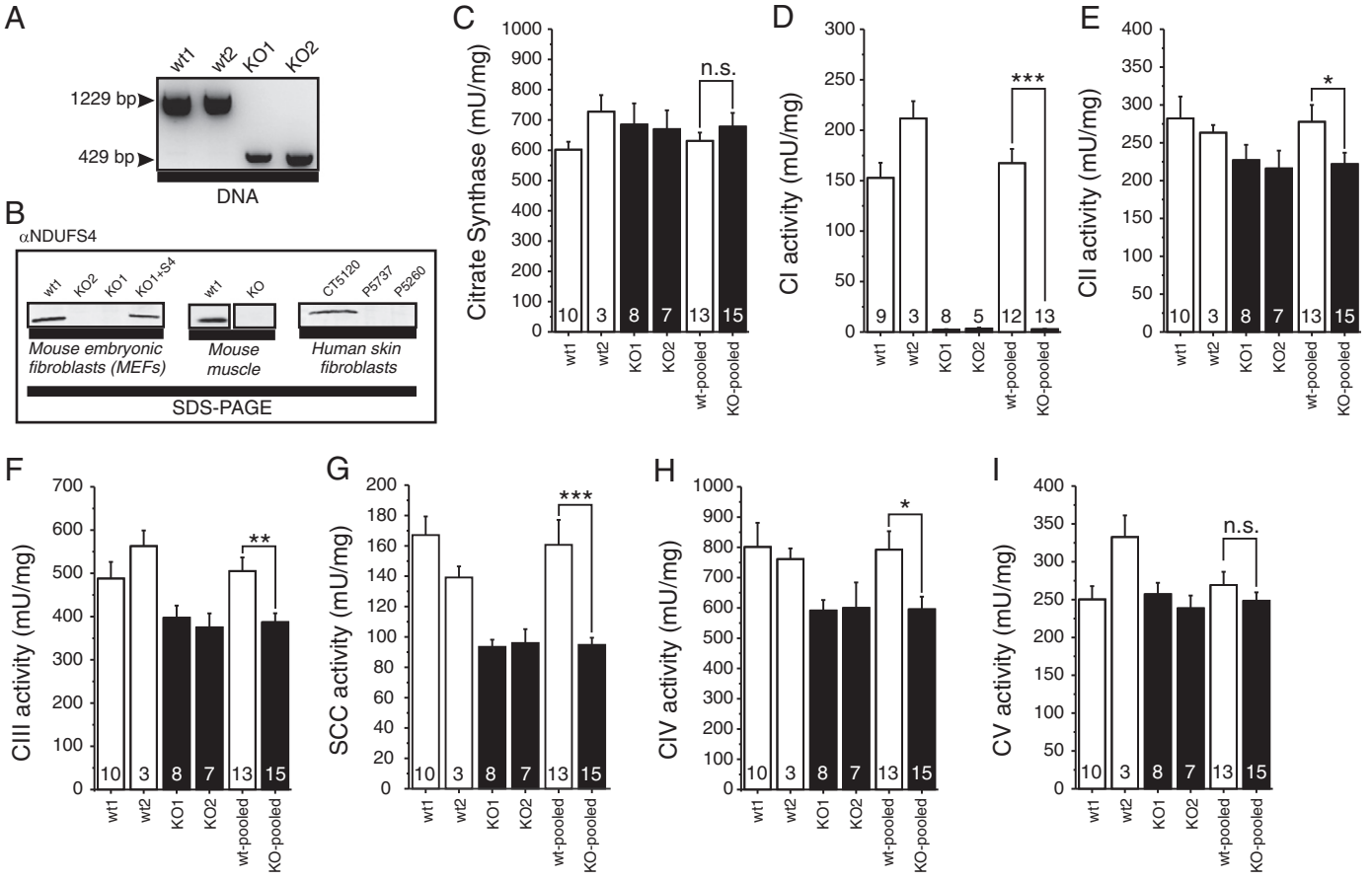

Fig. 1. NDUFS4 protein expression and maximal activity of OXPHOS complexes in wt and KO cells. (A) PCR analysis of the NDUFS4 subunit in two different wt (wt1, wt2) and KO (KO1, KO2) MEF cell lines. Wt cells display a band at 1229 bp, whereas KO cells display a band at 429 bp (the NDUFS4 subunit corresponds to 800 bp). (B) Left panel: SDS-PAGE analysis of NDUFS4 protein expression in mitochondrial fractions from wt (wt1), KOs (KO1, KO2) and complemented KO MEFs (KO1 + S4). Middle panel: a similar analysis in muscle cells. Right panel: a similar analysis comparing control (CT5120) and patient skin fibroblasts carrying an NDUFS4 mutation (P5737, P5260). (C) Maximal citrate synthase (CS) activity in mitoplasts from wt and KO MEFs. (D) Similar to panel C but now for maximal CI activity. (E) Similar to panel C but now for maximal CII activity. (F) Similar to panel C but now for maximal CIII activity. (G) Similar to panel C but now for maximal SCC (succinate-cytochrome *c* reductase) activity, a measure of the combined maximal activity of CII and CIII. (H) Similar to panel C but now for maximal CIV activity. (I) Similar to panel C but now for maximal CV activity. In this figure, numerals represent the number of assays performed on at least 2 different days. Statistical analysis was performed on the pooled data from wt (wt1 + wt2) and KO cells (KO1 + KO2). Significant differences between wt and KO cells are marked by *($p<0.05$), **($p<0.01$) and ***($p<0.001$). Abbreviations: n.s., not significant; KO, NDUFS4 knockout MEFs; S4, transfected with an NDUFS4-containing vector; wt, wildtype.

3.3. Mitochondria isolated from KO cells lack fully assembled CI on native gels

Blue native (BN)-PAGE analysis (Fig. 2A) revealed that wt MEFS expressed the fully-assembled 1000 kDa CI holocomplex (marked "CI"). Instead of holo-CI, KO MEFs contained a CI subassembly of smaller size (~830 kDa; marked "a"). *NDUFS4* gene deletion did not noticeably alter the levels of fully-assembled CII, CIII, CIV and CV. In-gel activity (IGA) analysis demonstrated that the ~830 kDa CI subassembly lacked CI activity (Fig. 2B; "KO1" and "KO2"). Reintroduction of the *NDUFS4* gene in the KO cells ("KO1 + S4" and "KO2 + S4") led to disappearance of the subassembly and reappearance of the fully assembled CI and IGA signal. Complementation of wt cells did not affect holo-CI expression and activity ("wt1 + S4"). Similarly, expression of an empty vector ("e") in wt ("wt1 + e") and KO cells ("KO1 + e" and "KO2 + e") was without effect. These results demonstrate that deletion of the *NDUFS4* gene does not affect the expression of fully-assembled CII, CIII, CIV and CV and is solely responsible for the altered CI assembly pattern and absence of CI activity in the KO cells.

3.4. Mitochondria isolated from KO cells contain an active ~200 kDa CI subassembly on native gels

We recently demonstrated the presence of an active ~200 kDa CI subassembly in kidney, brain, liver, lung, heart and muscle tissue of KO mice [42]. This subassembly, represents the NADH dehydrogenase module of CI and at least contains the NDUFV1 and NDUFV2 subunits of CI. Here we also detected the ~200 kDa CI subassembly in KO cells (Fig. 2C, marked "b"), which disappeared on complementation with the NDUFS4 subunit ("KO1 + S4").

3.5. Intact KO cells display a reduced oxygen consumption, which is fully inhibited by the specific CI inhibitor rotenone

Given the reduced maximal activities of CI–CIV (Fig. 1), we next investigated oxygen (O_2) consumption in intact cells to obtain a measure of mitochondrial functional capacity. *NDUFS4* gene deletion significantly reduced routine cellular O_2 consumption (Fig. 3A). This reduction was fully restored by *NDUFS4* gene complementation ("KO1 + S4"). Acute application of the specific CI inhibitor rotenone (ROT; 0.5 μM) directly inhibited cellular O_2 consumption (Fig. 3B–C). The latter was not reduced further by application of the CIII inhibitor antimycin A (AA; 2.5 μM; Fig. 3B–C). Cellular "leak" O_2 consumption (determined by application of the CV-inhibitor oligomycin (OLI; 2.5 μM)) and minimal O_2 consumption (determined by application of OLI, the mitochondrial uncoupler FCCP (3.5 μM), ROT and AA) were similar for KO and wt MEFs (Fig. 3D). Maximum cellular O_2 consumption (determined in the presence of OLI and FCCP) tended to be lower in KO cells. These findings demonstrate that intact KO cells display a substantial routine/maximal O_2 consumption that is lower than that in wt cells and completely and acutely blocked by ROT.

3.6. Total NAD^+ is decreased and total NADH is increased in KO cell homogenates

Previous live-cell microscopy analysis revealed that mitochondrial NAD(P)H levels are increased in fibroblasts from CI-deficient patients [16,37]. Here we observed that mitochondrial NAD(P)H autofluorescence was also increased in living KO MEFs (Fig. 4A). Quantification of total NAD^+, NADH, $NADP^+$ and NADPH levels in whole cell homogenates revealed that the [NAD^+] was reduced, whereas the [NADH] was increased in KO cells (Fig. 4B). The latter was paralleled by a slight increase in the levels of $NADP^+$ and NADPH. The ratio between the oxidized and reduced forms of nicotinamide adenine dinucleotide ([NAD^+]/[NADH]) is an important component of the cellular redox state. In KO cells, this ratio was ~2-fold lower (i.e. more reduced) than in wt cells (Fig. 4C). In contrast, the ratio between [$NADP^+$] and [NADPH] was not affected in KO cells. These findings suggest that CI-mediated NADH oxidation in KO cells is less efficient than in wt cells, inducing a reduction in [NAD^+]/[NADH] ratio. In human skin fibroblasts, evidence was provided that an elevated cytosolic/mitochondrial [NAD^+]/[NADH] ratio is linked to increased extracellular lactate levels [43]. Following 72 h of culturing, the culture medium of KO cells contained more lactate than that of wt cells (Fig. 4D) but a similar amount of glucose (Fig. 4E). In contrast to fibroblasts from CI-deficient patients [44], oxidation of the reactive oxygen species (ROS) reporter hydroethidine (HEt) was not increased in KO cells (Fig. 4F). The latter suggests that *NDUFS4* gene deletion does not increase ROS levels.

3.7. KO cells display normal expression of hexokinase I/II and phosphorylated pyruvate dehydrogenase

Although glucose levels were similar in the culture medium of wt and KO MEFs, the reduced mitochondrial O_2 consumption, the increased [NAD^+]/[NADH] ratio and the elevated lactate levels suggest that glycolysis is enhanced in KO cells relative to wt cells [45,46]. The mitochondrial association of hexokinase (HK) was demonstrated to

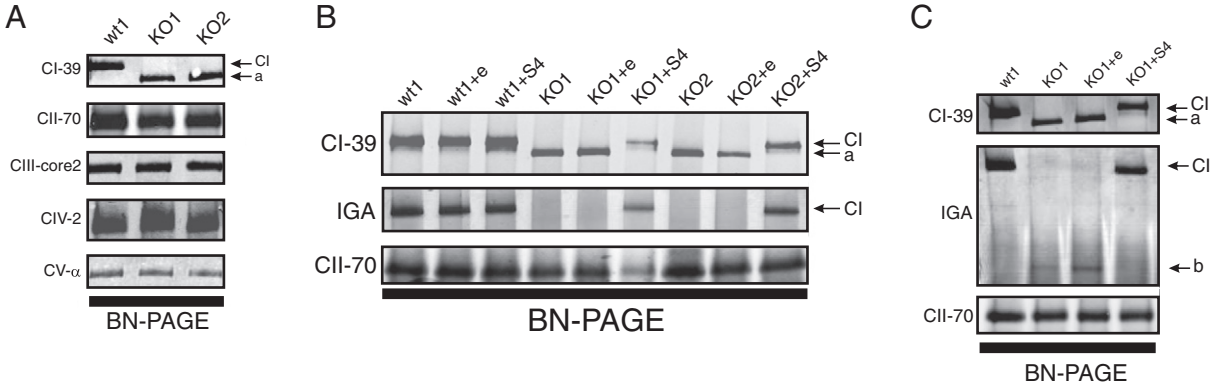

Fig. 2. BN-PAGE and in-gel activity analysis of wt and KO cells. (A) Arrows indicate the position of fully assembled CI ("CI") and the ~830 kDa CI subassembly ("a") in mitochondria-enriched fractions, as detected using an antibody against the 39-kDa (NDUFA9) subunit of CI (top row: "CI-39"). Subsequent panels depict the expression of fully-assembled CII ("CII-70"), CIII ("CIII-core2"), CIV ("CIV-2") and CV ("CV-α"). (B) The top row is similar to that in panel A. The middle row depicts the in-gel activity (IGA) signal of CI. The levels of fully-assembled CII (using an antibody against the 70-kDa subunit of CII) serve as a loading control (bottom row). (C) The top row is similar to that in panel A. The middle row depicts the in-gel activity (IGA) signal of CI, but now for a larger part of the gel. An active 200 kDa CI subassembly was detected (marked "b"). The levels of fully-assembled CII (using an antibody against the 70-kDa subunit of CII) serve as a loading control (bottom row). Abbreviations: e, transfected with an empty vector; KO, NDUFS4 knockout MEFs; S4, transfected with an NDUFS4-containing vector; wt, wildtype MEFs.

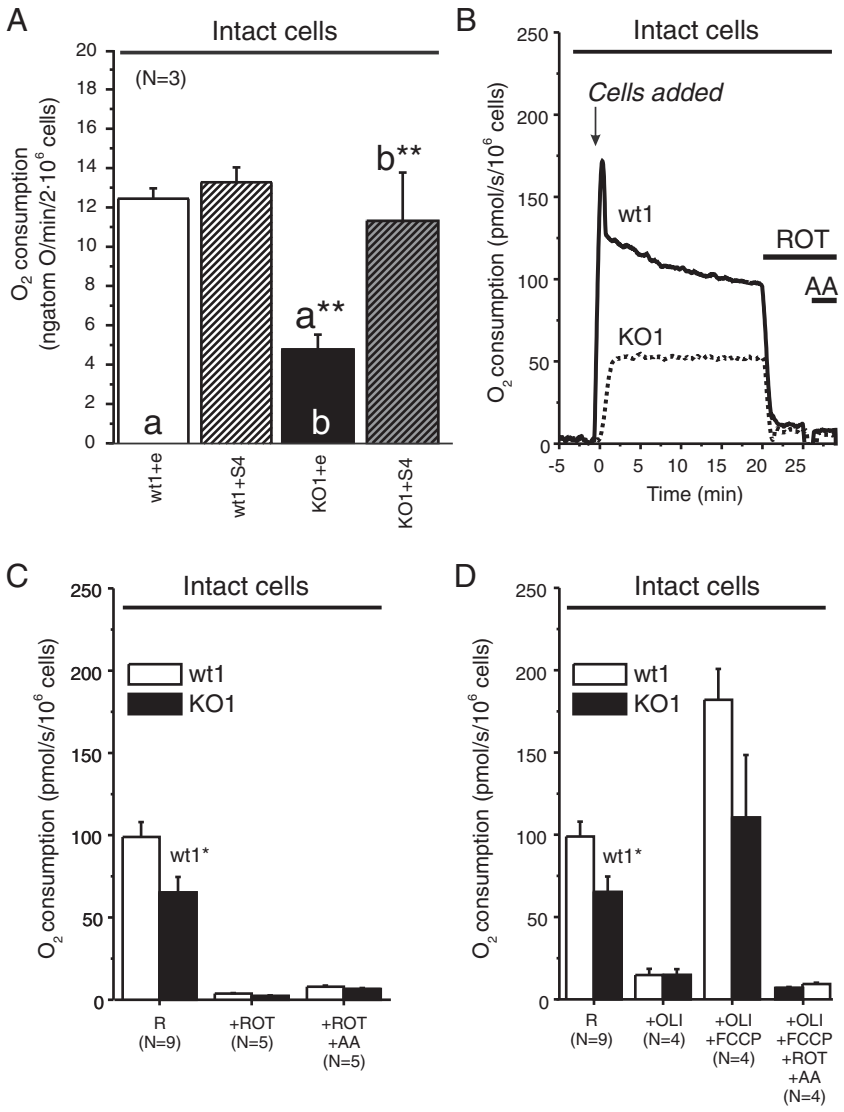

Fig. 3. O_2 consumption in intact wt and KO cells. (A) Average routine O_2 consumption in (complemented) wt and KO MEFs. (B) Typical example of reduced routine O_2 consumption in KO (KO1) vs. wt (wt1) MEFs. Addition of the specific complex I (CI) inhibitor rotenone (ROT) acutely inhibited O_2 consumption to the minimum level. (C) Average results obtained using the protocol in panel B. (D) Routine O_2 consumption (R) and the effect thereupon of subsequent application of OLI, FCCP, and ROT + AA. In this figure, routine O_2 consumption (R) for wt1 and KO1 (panels C and D) was calculated from the same 9 experiments and therefore identical. Numerals ("N") represent the number of experiments performed on at least 2 different days. Significant differences with the indicated conditions are marked by *($p<0.05$) and **($p<0.01$). Abbreviations: AA, antimycin A; e, transfected with an empty vector; FCCP, carbonylcyanide-p-trifluoromethoxyphenylhydrazone; KO, NDUFS4 knockout MEFs; OLI, oligomycin; ROT, rotenone; S4, transfected with an NDUFS4-containing vector; wt, wildtype MEFs.

enhance the flux through glycolysis [47]. However, Western blot analysis revealed that the protein levels of HKI (Fig. 5A, E) and HK-II (Fig. 5B, F) were not altered in KO cells, suggesting that *NDUFS4* gene deletion does not up regulate the glycolysis pathway. Next, we investigated the levels of phosphorylated pyruvate dehydrogenase (P-PDH) in mitochondrial fractions. PDH phosphorylation decreases the pyruvate flux into the TCA cycle, which promotes pyruvate conversion to lactate (i.e., aerobic glycolysis; [47]). Also the level of P-PDH (Fig. 5C, G) was not affected by *NDUFS4* gene deletion. Taken together, the results described in this paragraph suggest that *NDUFS4* gene deletion does not trigger a major up regulation of glycolysis.

3.8. KO cells display normal total cellular and free cytosolic ATP levels and a normal growth rate

Total cellular ATP content was not affected in KO cells (Fig. 6A). Similarly, analysis of the free cytosolic [ATP] using the proteinaceous ATP sensor "ATeam", revealed no detectable differences (Fig. 6B). Also the growth rate of the cells did not significantly differ between wt and KO MEFs (Fig. 6C). When extracellular glucose was replaced by the glycolysis inhibitor 2-deoxy-D-glucose (2-DG), which enters the cell via the glucose transporters on the plasmamembrane, the free cytosolic [ATP] concentration decreased with a similar rate in KO and wt cells (Fig. 6D, E, F). These findings demonstrate that the reduction in ETC activity (Fig. 1) and O_2 consumption (Fig. 3) does not detectably disturb ATP homeostasis and cell growth. Moreover, the results obtained with 2-DG suggest that the contribution of glycolysis-derived ATP to the resting free cytosolic [ATP] is similar in wt and KO cells. This supports our above conclusion that *NDUFS4* gene deletion does not trigger a major up regulation of glycolysis.

3.9. KO cells display increased mitochondrial TMRM fluorescence that is insensitive to oligomycin

The mitochondrial fluorescence signal of the cation TMRM (tetramethyl rhodamine methyl ester) was slightly higher in KO cells than in wt cells (Fig. 6G), suggesting hyperpolarization of the mitochondrial membrane potential ($\Delta\psi$). The latter was not maintained by

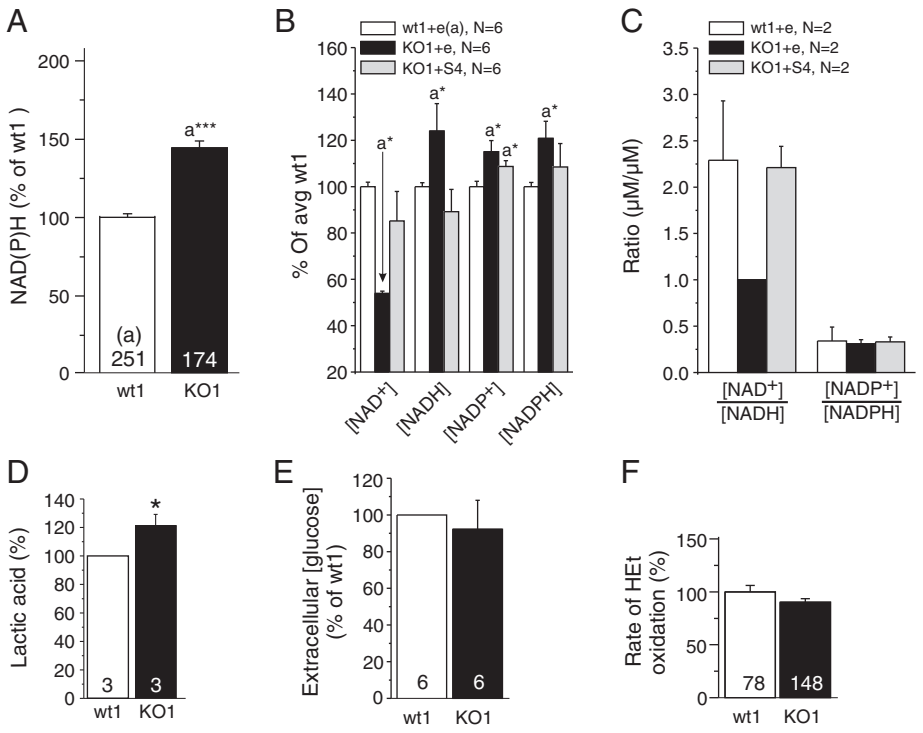

Fig. 4. NAD^+, NADH, $NADP^+$ and NADPH levels in wt and KO cells. (A) Mitochondrial NAD(P)H autofluorescence analyzed by live-cell microscopy. (B) Total levels of NAD^+, NADH, $NADP^+$ and NADPH in cell homogenates. (C) Ratios between total cellular [NAD^+] and [NADH], and between[$NADP^+$] and [NADPH]. (D) Levels of lactic acid in the medium after 72 h of cell culture. (E) Levels of glucose in the medium after 72 h of cell culture. (F) Rate of hydroethidine (HEt|) oxidation analyzed by live-cell microscopy. Significant differences with the indicated columns are marked by *($p<0.05$) and ***($p<0.001$). Numerals ("N") indicate the number of cells (panel A, F), assays (panels B, C, D and E) analyzed on at least two different days. The error bars (panels B, C) represent standard deviation. Abbreviations: e, transfected with an empty vector; KO, NDUFS4 knockout; S4, transfected with an NDUFS4-containing vector; wt, wildtype.

reverse-mode action of mitochondrial CV (F_oF_1-ATPase), since incubation of the cells with the CV-inhibitor oligomycin did not affect the mitochondrial TMRM staining pattern (Fig. 6H; 48). Quantitative analysis further revealed no oligomycin-induced translocation of TMRM from the mitochondrial compartment into the cell nucleus (Fig. 6I). These results suggest that *NDUFS4* gene deletion induces a

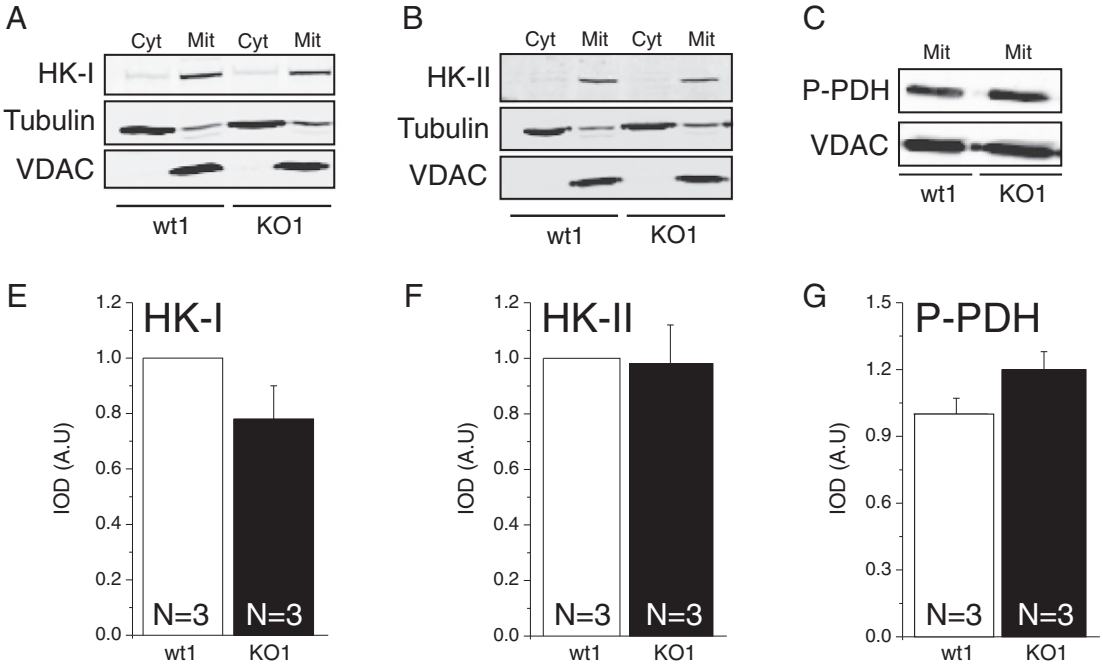

Fig. 5. Expression of key glycolytic enzymes in wt and KO cells. (A) Typical Western blot analysis of cytosolic (Cyt) and mitochondrial (Mit) fractions with respect to hexokinase I (HK-I). Tubulin and VDAC (voltage-dependent anion channel) were used as markers of the cytosolic and mitochondrial compartments, respectively. (B) Same as panel A but now for hexokinase II (HK-II). (C) Typical Western blot analysis of phosphorylated pyruvate dehydrogenase (P-PDH) in mitochondria-enriched fractions. (E) Quantification of HK-I Western blots. (F) Quantification of HK-II Western blots. (G) Quantification of P-PDH Western blots. Numerals ("N") indicate the number of independent experiments. Abbreviations: KO, NDUFS4 knockout; wt, wildtype.

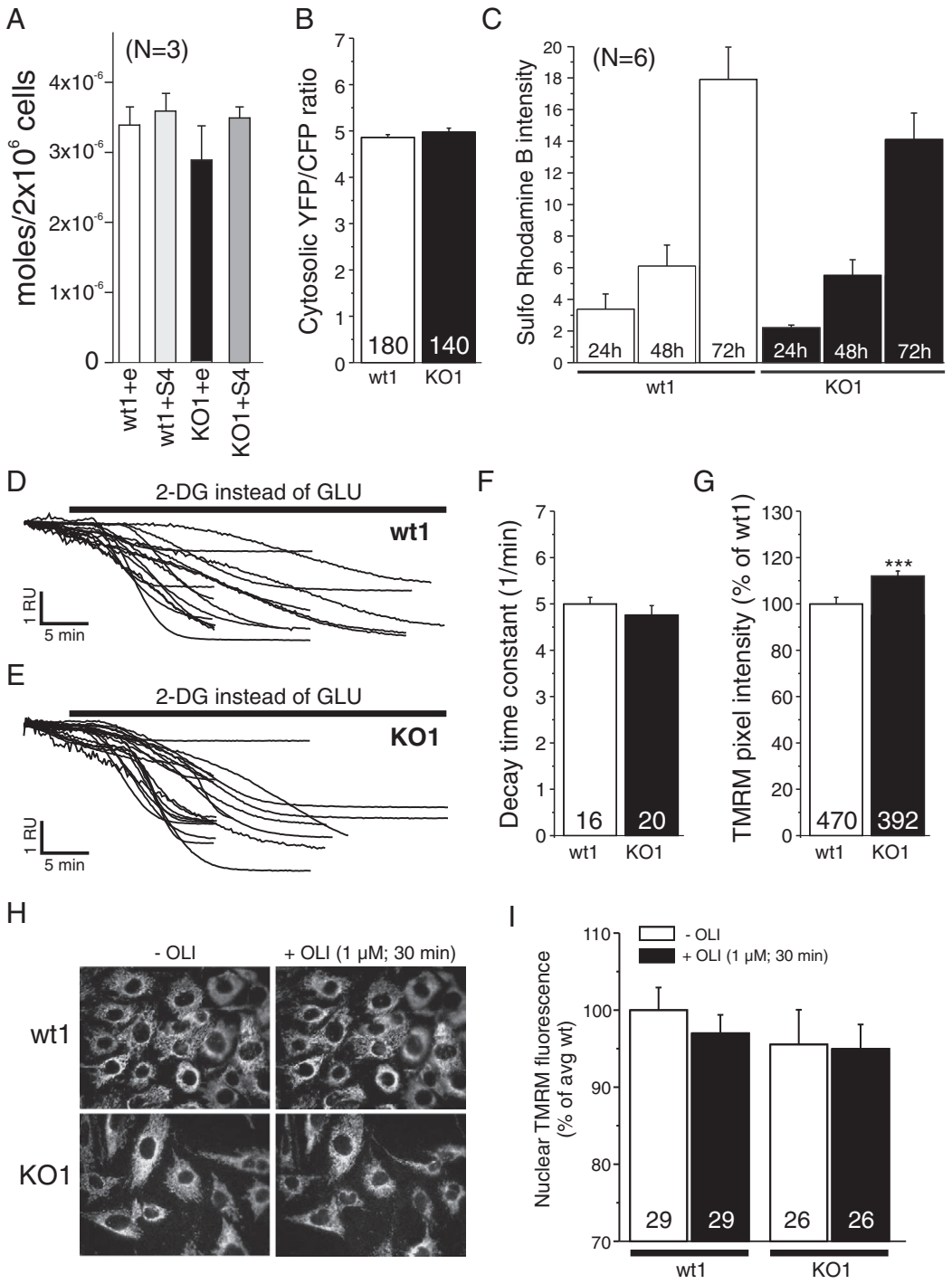

Fig. 6. Total cellular ATP amount and cytosolic free [ATP], mitochondrial TMRM fluorescence and effect of oligomycin thereupon in wt and KO cells. (A) Total ATP levels in whole cell homogenates. (B) Emission ratio (YFP/CFP) of the fluorescent ATP sensor ATeam in the cytosol. (C) Total cell number in wt and KO cell cultures at different time points. (D) Time-dependent effect of replacement of extracellular glucose (GLU) by an equimolar amount of the glycolysis inhibitor 2-deoxy-D-glucose (2-DG) on the ATeam emission ratio in wt MEFs. (E) Same as panel D but now for KO MEFs. (F) Decay time-constant of the traces in panels D and E, as determined by a mono-exponential fit ($R>0.96$). (G) Intensity of mitochondrial TMRM staining. (H) Lack of effect of the CV (F_oF_1-ATPase) inhibitor oligomycin (OLI) on the mitochondrial TMRM staining pattern. (I) Lack of effect of oligomycin (OLI) on the nuclear TMRM signal. In this figure, numerals ("N") represent the number of cell cultures (panels A and C) or cells (other panels) analyzed on at least 2 different days. Significant differences between wt and KO cells are indicated by ***($p<0.001$). Abbreviations: e, transfected with an empty vector; KO, NDUFS4 knockout; S4, transfected with an NDUFS4-containing vector; wt, wildtype.

slight mitochondrial hyperpolarization and that CV-reverse mode action is absent in wt and KO MEFs.

4. Discussion

Isolated mitochondrial CI deficiency is one of the most common OXPHOS deficiencies for which currently no cure is available [2,3,8,9,15]. Until recently, there was no good animal model for isolated human CI deficiency. Therefore, we and others used patient-derived primary skin fibroblasts for diagnostic, genetic and cell (patho)biological analyses (e.g. [14,19,24,37,40,44,49–51]). Here we determined the cell metabolic effects of *NDUFS4* gene deletion by comparing immortalized mouse embryonic fibroblasts (MEFs) from wildtype (wt) and *NDUFS4*$^{-/-}$ (KO) mice. These mice suffer from a

progressive fatal encephalomyopathy and represent the first animal model for isolated CI deficiency in humans [25].

4.1. NDUFS4 gene deletion induces CI destabilization

Western blot analysis revealed that mitochondria-enriched fractions from KO MEFs did not contain detectable amounts of NDUFS4 protein. This is compatible with the fact that deletion of exon 2 of the *NDUFS4* gene precludes synthesis of mature NDUFS4 protein [25]. Analysis of mitoplast fractions demonstrated that *NDUFS4* gene deletion reduces the maximal activity (V_{max}) of all ETC complexes to a greater (CI) or lesser (CII–CIV) extent, whereas CS and CV activities are not affected. Previous V_{max} analysis in patient fibroblasts with *NDUFS4* mutations revealed a variety of results including: (i) reduced CI activity and normal CIV activity [18], (ii) reduced CI and reduced CIII activity [20], (iii) reduced CI and normal CIII activity [52], (iv) reduced CI and reduced CIII [53], and (v) reduced CI, normal CIV and a slightly reduced CIII activity [54]. On native gels, fully-assembled CI was not detected and expression of fully assembled CII, CIII, CIV and CV was normal in mitochondrial fractions isolated from KO cells. Compatible with our result, it was demonstrated previously that CIII stability is not affected by the absence of CI [55]. Our findings suggest that *NDUFS4* gene deletion greatly destabilizes CI and thereby also induces minor catalytic defects in the other ETC complexes. The latter probably relates to the observation that OXPHOS complexes are organized in supercomplexes that contain CI, CIII and CIV and possibly also CII [56]. In this sense, the presence of the NDUFS4 protein and/or fully-assembled CI might be required for activity regulation of CII–CIV in intact cells.

In case of CI, native gel electrophoresis revealed that KO MEFs contain two CI subassemblies with a size of ~830 kDa and ~200 kDa instead of the fully-assembled complex (~1000 kDa). In-gel activity analysis demonstrated that the ~200 kDa subassembly was active whereas the ~830 kDa subassembly was not. Previous analysis of primary skin fibroblasts from patients with an *NDUFS4* mutation also revealed an inactive ~830 kDa subcomplex [15,53]. However, in contrast to KO MEFs, mitoplast fractions of patient cells displayed considerable CI activity (V_{max}) in biochemical assays. This led us to propose that the primary role of the NDUFS4 subunit is a regulatory one by controlling the stability and, thus, the cellular expression of the active complex [15], supporting a function for NDUFS4 in regulation of CI activity [23,24]. In a parallel study, we recently analyzed the nature and penetrance of the CI deficiency in primary tissues (pancreas, kidney, liver, lung, brain, heart and muscle) from the KO animal [42]. This analysis revealed that: (i) CI activity is reduced but not abolished by *NDUFS4* gene deletion, (ii) the diverse tissues contained both a ~830 kDa and an (active) ~200 kDa subassembly, (iii) the ~830 kDa CI subassembly lacks the tip (i.e. the ~200 kDa subassembly) of CI, and that this tip represents the NADH dehydrogenase module. We proposed a model in which CIII stabilizes CI in the absence of NDUFS4 to allow formation of active CI in the diverse tissues of the KO animal [42].

Here we observed that routine and maximal O_2 consumptions were reduced in intact KO MEFs. Interestingly, respiration was immediately and fully inhibited by acute application of the specific CI inhibitor rotenone. These results are compatible with the lower V_{max} of the ETC complexes and demonstrate that catalytically active CI is present in the KO cells, supporting our above results obtained in KO mouse tissues. The fact that oxygen consumption was completely inhibited in rotenone-treated MEFs further suggests that CII-mediated succinate oxidation is not of major importance in these cells. This might indicate that succinate levels are low and/or the rotenone induced increase in the level of mitochondrial NADH, a known inhibitor of the TCA cycle, prevents succinate oxidation by CII (which also constitutes part of the TCA cycle).

Importantly, OXPHOS complexes display a tissue-dependent stoichiometry, possibly affecting their (supercomplex-mediated) stability [2]. Moreover, analysis of cell homogenates, mitochondria-enriched fractions and mitoplasts requires the use of detergents and/or permeabilization agents. Since these disrupt mitochondrial structure and function, direct comparison with live-cell experiments becomes difficult [57]. Therefore the various CI activity values obtained in the diverse cells and tissues (and perhaps also the activities of other ETC complexes), are subject to variations in ETC stoichiometry and sample preparation, leading to different amounts of functional enzyme due to CI instability, caused by the absence of NDUFS4 [15,25,42]. This provides a potential explanation for the fact that living KO cells display CI-dependent O_2 consumption, whereas fully-assembled and active CIs were not detected by native gel and biochemical analysis.

4.2. NDUFS4 gene deletion elevates [NAD^+]/[NADH] ratio and lactate production

NDUFS4 KO cells displayed an increased mitochondrial NAD(P)H autofluorescence. A similar increase was previously observed in patient-derived primary fibroblasts carrying various *NDUFS4* mutations [37,44,58]. Since autofluorescence microscopy analysis cannot discriminate between NADH and NADPH we also analyzed whole cell homogenates and demonstrated that the cellular [NAD^+]/[NADH] ratio was increased whereas the [$NADP^+$]/[NADPH] ratio was normal in the KO cells. These results indicate that CI malfunction is associated with increased cellular NADH levels. Given the previously reported link between elevated cytosolic/mitochondrial [NAD^+]/[NADH] ratio and extracellular lactate levels [43], we also quantified lactic acid levels in the culture medium. This revealed a 20% higher value in medium from KO cells, following 72 h of culturing. Given the fact that the number of cells was ~22% less and glucose levels were ~8% lower in KO cell cultures, this suggests that KO cells are (slightly) more glycolytic than wt cells.

4.3. NDUFS4 gene deletion does not induce a major switch toward a more glycolytic cellular phenotype

Tumor cells known to be highly glycolytic, display increased expression of glycolytic enzymes, including hexokinases (HKs; [60]). HKs catalyze the first step of the glycolysis (i.e. the conversion of glucose into glucose 6-phosphate; [39,47]). Similarly, upregulation of aerobic glycolysis has been linked to inactivation of pyruvate dehydrogenase (PDH; [61]). PDH constitutes part of the pyruvate dehydrogenase complex (PDC) located inside mitochondria and converts pyruvate generated by the glycolysis into the TCA-cycle substrate acetyl-CoA. Reversible phosphorylation of PDH acts as inhibitory and decreases pyruvate flux into the TCA cycle, which promotes pyruvate conversion to lactate [47]. PDH phosphorylation occurs at three sites on the E1 alpha subunit of PDH (PDHE1α: Ser^{232}, Ser^{293} and Ser^{300}) and phosphorylation at any one site leads to inhibition of the complex in vitro [62]. Wt and KO MEFs displayed similar protein levels of HK-I, HK-II and P-PDH. This argues against the idea that *NDUFS4* gene knockout triggers a major upregulation of the glycolytic pathway in KO cells. However, spontaneously immortalized MEFs already display a high glycolytic activity that also appears to protect from oxidative damage [59]. Moreover, spontaneous cell immortalization has been associated with resistance to ROS-induced growth arrest [63] and upregulation of oxidative stress pathway genes in primary breast tumors [64]. This not only provides a plausible explanation for the fact that oxidation of the ROS sensor hydroethidine (HEt) was not increased in KO cells, but also suggests that a further upregulation of glycolysis in NDUFS4 KO cells is unnecessary to sustain cell function.

4.4. NDUFS4 gene deletion does not detectably affect total and free cytosolic ATP levels

Although routine O_2 consumption was reduced in KO cells, total cellular ATP content and free cytosolic [ATP] in resting cells were not affected by *NDUFS4* deletion. This suggests that the latter does not detectably affect the balance between total cellular ATP production and consumption. Cytosolic free [ATP] decayed at equal rates when extracellular glucose was removed and replaced by the glycolysis-inhibitor 2-DG. We conclude from this data that *NDUFS4* gene deletion does not detectably alter the glycolysis-mediated ATP generation pathway, further supporting our above conclusion that *NDUFS4* gene deletion does not upregulate glycolysis. CV inhibition by oligomycin did not affect mitochondrial TMRM localization, arguing against reverse-mode action of CV previously observed in glycolytic cells [65] and cells with mtDNA mutations [48]. KO cells displayed a mildly increased mitochondrial TMRM fluorescence, suggestive of $\Delta\psi$ hyperpolarization. A similar increase was observed in fibroblasts from patients with a TMEM70 mutation, which displayed a reduced expression and maximal activity of CV [66]. $\Delta\psi$ hyperpolarization in glycolytic cells has been taken as evidence of reduced ATP utilization [67]. This suggests that KO cell growth is slightly reduced and glycolysis in the KO cells is slightly stimulated to compensate for the loss in mitochondrial ATP producing capacity.

5. Conclusion

Taken together, our data support a mechanism in which *NDUFS4* gene deletion induces CI destabilization leading to a reduction in ETC function and mitochondrial O_2 consumption. Given the metabolic properties of immortalized MEFs (e.g. their high glycolytic rate), alterations in cell metabolism induced by mitochondrial dysfunction might be difficult to detect. This is illustrated by the (very) slight shift toward a more glycolytic phenotype and our failure to demonstrate increased ROS levels in the KO MEFs. In this sense, immortalized cells and/or high-glucose culture conditions might not be ideal to study the (patho)physiology of mitochondrial (dys)function. To address this issue wt and KO MEFs, as well as primary cells, cultured under low extracellular glucose or galactose conditions, are currently analyzed in our laboratory.

Acknowledgements

This work was supported by an equipment grant of NWO (Netherlands Organization for Scientific Research, No: 911-02-008), a grant of the 'Prinses Beatrix Fonds' (No: OP-05-04) and by the CSBR (Centres for Systems Biology Research) initiative from the Netherlands Organisation for Scientific Research (NWO; No: CSBR09/013V). We thank Dr. R. Palmiter (Howard Hughes Medical Institute and Department of Biochemistry, University of Washington, Seattle, WA, USA) for providing the *NDUFS4*$^{-/-}$ mouse, Mr. A Klymov for assistance with the ATeam measurements and Mr. G. Manjeri for PCR analysis.

References

[1] C.E.J. Dieteren, S.C. Gielen, L.G.J. Nijtmans, J.A.M. Smeitink, H.G. Swarts, R. Brock, P.H.G.M. Willems, W.J.H. Koopman, Solute diffusion is hindered in the mitochondrial matrix, Proc. Natl. Acad. Sci. U.S.A. 108 (2011) 8657–8662.
[2] W.J.H. Koopman, L.G. Nijtmans, C.E. Dieteren, P. Roestenberg, F. Valsecchi, J.A.M. Smeitink, P.H.G.M. Willems, Mammalian mitochondrial complex I: biogenesis, regulation, and reactive oxygen species generation, Antioxid. Redox Signal. 12 (2010) 1431–1470.
[3] J.A.M. Smeitink, L. van den Heuvel, S. DiMauro, The genetics and pathology of oxidative phosphorylation, Nat. Rev. Genet. 2 (2001) 342–352.
[4] C.J. Dunning, M. McKenzie, C. Sugiana, M. Lazarou, J. Silke, A. Connelly, J.M. Fletcher, D.M. Kirby, D.R. Thorburn, M.T. Ryan, Human CIA30 is involved in the early assembly of mitochondrial complex I and mutations in its gene cause disease, EMBO J. 26 (2007) 3227–3237.
[5] M. Lazarou, M. McKenzie, A. Ohtake, D.R. Thorburn, M.T. Ryan, Analysis of the assembly profiles for mitochondrial- and nuclear-DNA-encoded subunits into complex I, Mol. Cell. Biol. 27 (2007) 4228–4237.
[6] M. Mimaki, X. Wang, M. McKenzie, D.R. Thorburn, M.T. Ryan, Understanding mitochondrial complex I assembly in health and disease, Biochim. Biophys. Acta 1817 (2012) 851–862.
[7] J. Nouws, L.G.J. Nijtmans, J.A.M. Smeitink, R.O. Vogel, Assembly factors as a new class of disease genes for mitochondrial complex I deficiency: cause, pathology and treatment options, Brain 135 (2012) 12–22.
[8] H. Pagniez-Mammeri, S. Loublier, A. Legrand, P. Bénit, P. Rustin, A. Slama, Mitochondrial complex I deficiency of nuclear origin I. Structural genes, Mol. Genet. Metab. 105 (2012) 163–172.
[9] H. Pagniez-Mammeri, H. Rak, A. Legrand, P. Bénit, P. Rustin, A. Slama, Mitochondrial complex I deficiency of nuclear origin II. Non-structural genes, Mol. Gen. Metab. 105 (2012) 163–172.
[10] R.O. Vogel, C.E.J. Dieteren, L.P. van den Heuvel, P.H.G.M. Willems, J.A.M. Smeitink, W.J.H. Koopman, L.G.J. Nijtmans, Identification of mitochondrial complex I assembly intermediates by tracing tagged NDUFS3 demonstrates the entry point of mitochondrial subunits, J. Biol. Chem. 282 (2007) 7582–7590.
[11] C.E.J. Dieteren, P.H.G.M. Willems, R.O. Vogel, H.G. Swarts, J. Fransen, R. Roepman, G. Crienen, J.A.M. Smeitink, L.G.J. Nijtmans, W.J.H. Koopman, Subunits of mitochondrial complex I exist as part of matrix- and membrane-associated subcomplexes in living cells, J. Biol. Chem. 283 (2008) 34753–34761.
[12] E. Perales-Clemente, E. Fernandez-Vizarra, R. Acin-Perez, N. Movilla, M.P. Bayona-Bafaluy, R. Moreno-Loshuertos, A. Perez-Martos, P. Fernandez-Silva, J.A. Enriquez, Five entry points of the mitochondrially encoded subunits in mammalian complex I assembly, Mol. Cell. Biol. 30 (2010) 3038–3047.
[13] C.E.J. Dieteren, P.H.G.M. Willems, H.G. Swarts, J. Fransen, J. Smeitink, W.J.H. Koopman, L.G.J. Nijtmans, Defective mitochondrial translation differentially affects the live cell dynamics of complex I subunits, Biochim. Biophys. Acta 1807 (2011) 1624–1633.
[14] E. Fassone, J.W. Taanman, I.P. Hargreaves, N.J. Sebire, M.A. Cleary, M. Burch, S. Rahman, Mutations in the mitochondrial complex I assembly factor NDUFAF1 cause fatal infantile hypertropic cardiomyopathy, J. Med. Genet. 48 (2011) 691–697.
[15] F. Valsecchi, W.J.H. Koopman, G.R. Manjeri, R.J. Rodenburg, J.A.M. Smeitink, P.H.G.M. Willems, Complex I disorders: causes, mechanisms, and development of treatment strategies at the cellular level, Dev. Disabil. Res. Rev. 16 (2010) 175–182.
[16] F. Distelmaier, W.J.H. Koopman, L.P. van den Heuvel, R.J. Rodenburg, E. Mayatepek, P.H.G.M. Willems, J.A.M. Smeitink, Mitochondrial complex I deficiency: from organelle dysfunction to clinical disease, Brain 132 (2009) 833–842.
[17] L.P. van den Heuvel, W. Ruitenbeek, R. Smeets, Z. Gelman-Kohan, O. Elpeleg, J. Loeffen, F. Trijbels, E. Mariman, D. de Bruijn, J.A.M. Smeitink, Demonstration of a new pathogenic mutation in human complex I deficiency: a 5-bp duplication in the nuclear gene encoding the 18-kDa (AQDQ) subunit, Am. J. Hum. Genet. 62 (1998) 262–268.
[18] V. Petruzzella, R. Vergari, I. Puzziferri, D. Boffoli, A. Lamantea, M. Zeviani, S. Papa, A nonsense mutation in the *NDUFS4* gene encoding the 18 kDa (AQDQ) subunit of complex I abolishes assembly and activity of the complex in a patient with Leigh-like syndrome, Hum. Mol. Genet. 10 (2001) 529–535.
[19] S.M. Budde, L.P. van den Heuvel, A.J. Jansen, R.J. Smeets, C.A. Buskens, L. DeMerleir, R. Baethmann, T. Voit, J.M. Trijbels, J.A.M. Smeitink, Combined enzymatic complex I and complex III deficiency associated with mutations in the nuclear encoded *NDUFS4* gene, Biochem. Biophys. Res. Commun. 18 (2000) 63–68.
[20] S.M. Budde, L.P. van den Heuvel, R.J. Smeets, D. Skladal, J.A. Mayr, C. Boelen, V. Petruzzella, S. Papa, J.A.M. Smeitink, Clinical heterogeneity in patients with mutations in the *NDUFS4* gene of mitochondrial complex I, J. Inherit. Metab. Dis. 26 (2003) 813–815.
[21] V. Petruzzella, S. Papa, Mutations in human nuclear genes encoding for subunits of mitochondrial respiratory complex I: the *NDUFS4* gene, Gene 286 (2002) 149–154.
[22] S. Papa, S. Scacco, A.M. Sardanelli, V. Petruzzella, R. Vergari, A. Signorile, Z. Techikova-Dobrova, Complex I and the cAMP cascade in human physiopathology, Biosci. Rep. 22 (2002) 3–16.
[23] D. De Rasmo, A. Signorile, F. Papa, E. Roca, S. Papa, cAMP/Ca^{2+} response element-binding protein plays a central role in the biogenesis of respiratory chain proteins in mammalian cells, IUBMB Life 62 (2010) 447–452.
[24] D. De Rasmo, A. Signorile, M. Larizza, C. Pacelli, T. Cocco, S. Papa, Activation of the cAMP cascade in human fibroblast cultures rescues the activity of oxidatively damaged complex I, Free. Rad. Biol. Med. 52 (2012) 757–764.
[25] S.E. Kruse, W.C. Watt, D.J. Marcinek, R.P. Kapur, K.A. Schenkman, R.D. Palmiter, Mice with mitochondrial complex I deficiency develop a fatal encephalomyopathy, Cell Metab. 7 (2008) 312–320.
[26] G.J. Todaro, H. Green, Quantitative studies of the growth of mouse embryo cells in culture and their development into established lines, J. Cell Biol. 17 (1963) 299–313.
[27] T.M. Kinsella, G.P. Nolan, Episomal vectors rapidly and stably produce high-titer recombinant retrovirus, Hum. Gene Ther. 7 (1996) 1405–1413.
[28] G.P. Nolan, A.R. Shatzman, Expression vectors and delivery systems, Curr. Opin. Biotechnol. 9 (1998) 447–450.
[29] F. Michiels, R.A. van der Kammen, L. Janssen, G. Nolan, J.G. Collard, Expression of Rho GTPases using retroviral vectors, Methods Enzymol. 325 (2000) 295–302.
[30] R.J. Rodenburg, Biochemical diagnosis of mitochondrial disorders, J. Inherit. Metab. Dis. 100 (2010) 283–292.

[31] A.J. Janssen, F.J. Trijbels, R.C. Sengers, J.A.M. Smeitink, L.P. van den Heuvel, L.T. Wintjes, B.J. Stoltenborg-Hogenkamp, R.J. Rodenburg, Spectrophotometric assay for complex I of the respiratory chain in tissue samples and cultured fibroblasts, Clin. Chem. 53 (2007) 729–734.
[32] R. Rossignol, R. Gilkerson, R. Aggeler, K. Yamagata, S.J. Remington, R.A. Capaldi, Energy substrate modulates mitochondrial structure and oxidative capacity in cancer cells, Cancer Res. 64 (2004) 985–993.
[33] N. Bellance, G. Benard, F. Furt, H. Begueret, K. Smolkova, E. Passerieux, J.P. Delage, J.M. Baste, P. Moreau, R. Rossignol, Bioenergetics of lung tumors: alteration of mitochondrial biogenesis and respiratory capacity, Int. J. Biochem. Cell Biol. 41 (2009) 2566–2577.
[34] E. Hutter, K. Renner, G. Pfister, P. Stockl, P. Jansen-Durr, E. Gnaiger, Senescence-associated changes in respiration and oxidative phosphorylation in primary human fibroblasts, Biochem. J. 380 (2004) 919–928.
[35] K. Wosikowski, K. Mattern, I. Schemainda, M. Hasmann, B. Rattel, R. Loser, WK175, a novel antitumor agent, decreases the intracellular nicotinamide adenine dinucleotide concentration and induces the apoptotic cascade in human leukemia cells, Cancer Res. 62 (2002) 1057–1062.
[36] J.C. Komen, F. Distelmaier, W.J.H. Koopman, R.J. Wanders, J.A.M. Smeitink, P.H.G.M. Willems, Phytanic acid impairs mitochondrial respiration through protonophoric action, Cell. Mol. Life Sci. 64 (2007) 3271–3281.
[37] S. Verkaart, W.J.H. Koopman, J. Cheek, S.E. van Emst-de Vries, L.W. van den Heuvel, J.A.M. Smeitink, P.H.G.M. Willems, Mitochondrial and cytosolic thiol redox state are not detectably altered in isolated human NADH:ubiquinone oxidoreductase deficiency, Biochim. Biophys. Acta 1772 (2007) 1041–1051.
[38] H. Imamura, K.P. Nhat, H. Togawa, K. Saito, R. Iino, Y. Kato-Yamada, T. Nagai, H. Noji, Visualization of ATP levels inside single living cells with fluorescence resonance energy transfer-based genetically encoded indicators, Proc. Natl. Acad. Sci. U.S.A. 106 (2009) 15651–15656.
[39] D.C. Liemburg-Apers, H. Imamura, M. Forkink, M. Nooteboom, H.G. Swarts, R. Brock, J.A.M. Smeitink, P.H.G.M. Willems, W.J.H. Koopman, Quantitative glucose and ATP sensing in mammalian cells, Pharm. Res. 28 (2011) 2745–2757.
[40] H.J. Visch, G.A. Rutter, W.J.H. Koopman, J.B. Koenderink, S. Verkaart, T. de Groot, A. Varadi, K.J. Mitchell, L.P. van den Heuvel, J.A.M. Smeitink, P.H.G.M. Willems, Inhibition of mitochondrial Na^{+}–Ca^{2+} exchange restores agonist-induced ATP production and Ca^{2+} handling in human complex I deficiency, J. Biol. Chem. 279 (2004) 40328–40336.
[41] F. Distelmaier, W.J.H. Koopman, E.R. Testa, A.S. de Jong, H.G. Swarts, E. Mayatepek, J.A.M. Smeitink, P.H.G.M. Willems, Life cell quantification of mitochondrial membrane potential at the single organelle level, Cytometry A 73 (2008) 129–138.
[42] M.A. Calvaruso, P.H.G.M. Willems, M. van den Brand, F. Valsecchi, S. Kruse, R. Palmiter, J.A.M. Smeitink, L.G.J. Nijtmans, Mitochondrial complex III stabilizes complex I in the absence of NDUFS4 to provide partial activity, Hum. Mol. Genet. 21 (2012) 115–120.
[43] F.A. Wijburg, N. Feller, W. Ruitenbeek, J.M. Trijbels, R.C. Sengers, H.R. Scholte, H. Przyrembel, R.J. Wanders, Detection of respiratory chain dysfunction by measuring lactate and pyruvate production in cultured fibroblasts, J. Inherit. Metab. Dis. 13 (1990) 355–358.
[44] S. Verkaart, W.J.H. Koopman, S.E. van Emst-de Vries, L.G.J. Nijtmans, L.W. van den Heuvel, J.A.M. Smeitink, P.H.G.M. Willems, Superoxide production is inversely related to complex I activity in inherited complex I deficiency, Biochim. Biophys. Acta 1772 (2007) 373–381.
[45] M.G. Vander Heiden, L.C. Cantley, C.B. Thompson, Understanding the Warburg effect: the metabolic requirements of cell proliferation, Science 324 (2009) 1029–1033.
[46] G. Benard, N. Bellance, C. Jose, S. Melser, K. Nouette-Gaulain, R. Rossignol, Multi-site control and regulation of mitochondrial energy production, Biochim. Biophys. Acta 1797 (2010) 698–709.
[47] S.Y. Lunt, M.G. Vander Heiden, Aerobic glycolysis: meeting the metabolic requirements of cell proliferation, Annu. Rev. Cell Dev. Biol. 27 (2011) 441–464.
[48] M. McKenzie, D. Liolitsa, N. Akinshina, M. Campanella, S. Sisodiya, I. Hargreaves, N. Nirmanalanthan, M.G. Sweeney, P.M. Abou-Sleiman, N.W. Wood, M.G. Hanna, M.R. Duchen, Mitochondrial *ND5* gene variation associated with encephalomyopathy and mitochondrial ATP consumption, J. Biol. Chem. 282 (2007) 36845–36852.
[49] W.J.H. Koopman, H.J. Visch, S. Verkaart, L.W. van den Heuvel, J.A.M. Smeitink, P.H.G.M. Willems, Mitochondrial network complexity and pathological decrease in complex I activity are tightly correlated in isolated human complex I deficiency, Am. J. Physiol. 289 (2005) C881–C890.
[50] S.J. Hoefs, C.E.J. Dieteren, F. Distelmaier, R.J. Janssen, A. Epplen, H.G. Swarts, M. Forkink, R.J. Rodenburg, L.G.J. Nijtmans, P.H.G.M. Willems, J.A.M. Smeitink, L.P. van den Heuvel, NDUFA2 complex I mutation leads to Leigh disease, Am. J. Hum. Genet. 82 (2008) 1306–1315.
[51] A. Saada, The use of individual patient's fibroblasts in the search for personalized treatment of nuclear encoded OXPHOS diseases, Mol. Genet. Metab. 104 (2011) 39–47.
[52] S. Scacco, V. Petruzzella, S. Budde, R. Vergari, R. Tamborra, D. Panelli, L.P. van den Heuvel, J.A. Smeitink, S. Papa, Pathological mutations of the human *NDUFS4* gene of the 18-kDa (AQDQ) subunit of complex I affect the expression of the protein and the assembly and function of the complex, J. Biol. Chem. 278 (2003) 44161–44167.
[53] C. Ugalde, R.J. Janssen, L.P. van den Heuvel, J.A.M. Smeitink, L.G.J. Nijtmans, Differences in assembly or stability of complex I and other mitochondrial OXPHOS complexes in inherited complex I deficiency, Hum. Mol. Genet. 13 (2004) 659–667.
[54] A. Iuso, S. Scacco, C. Piccoli, F. Bellomo, V. Petruzzella, R. Trentadue, M. Minuto, M. Ripoli, N. Capitanio, M. Zeviani, S. Papa, Dysfunctions of cellular oxidative metabolism in patients with mutations in the *NDUFS1* and *NDUFS4* genes of complex I, J. Biol. Chem. (2006) 10347–10380.
[55] R. Acin-Pérez, M.P. Bayona-Bafaluy, P. Fernandez-Silva, R. Moreno-Loshuertos, A. Perez-Martos, C. Bruno, C.T. Moraes, J.A. Enriquez, Respiratory complex III is required to maintain complex I in mammalian mitochondria, Mol. Cell 13 (2004) 805–815.
[56] N.V. Dudkina, R. Kouril, K. Peters, H.P. Braun, E.J. Boekema, Structure and function of mitochondrial supercomplexes, Biochim. Biophys. Acta 1797 (2010) 664–670.
[57] M. Picard, Taivassalo, D. Ritchie, K.J. Wright, M.M. Thomas, C. Romestaing, R.T. Hepple, Mitochondrial structure and function are disrupted by standard isolation methods, PLoS One 6 (2011) e18317.
[58] W.J.H. Koopman, S. Verkaart, H.J. Visch, S. van Emst-de Vries, L.G.J. Nijtmans, J.A.M. Smeitink, P.H.G.M. Willems, Human NADH:ubiquinone oxidoreductase deficiency: radical changes in mitochondrial morphology? Am. J. Physiol. 293 (2007) C22–C29.
[59] H. Kondoh, M.E. Lleonart, D. Bernard, J. Gil, Protection from oxidative stress by enhanced glycolysis; a possible mechanism of cellular immortalization, Histol. Histopathol. 22 (2007) 85–90.
[60] T.A. Smith, Mammalian hexokinases and their abnormal expression in cancer, Br. J. Biomed. Sci. (2000) 170–178.
[61] T. Hitosugi, J. Fan, T.W. Chung, K. Lythgoe, X. Wang, J. Xie, Q. Ge, T.L. Gu, R.D. Polakiewicz, J.L. Roesel, G.Z. Chen, T.J. Boggon, S. Lonial, H. Fu, F.R. Khuri, S. Kang, J. Chen, Tyrosine phosphorylation of mitochondrial pyruvate dehydrogenase kinase 1 is important for cancer metabolism, Mol. Cell 44 (2011) 864–877.
[62] M.J. Rardin, S.E. Wiley, R.K. Naviaux, A.N. Murphy, J.E. Dixon, Monitoring phosphorylation of the pyruvate dehydrogenase complex, Anal. Biochem. 389 (2009) 157–164.
[63] A.L. Fridman, M.A. Tainsky, Critical pathways in cellular senescence and immortalization revealed by gene expression profiling, Oncogene 27 (2008) 5975–5987.
[64] S.H. Dairkee, M. Nicolau, A. Sayeed, S. Champion, Y. Yi, D.H. Moore, B. Yong, Z. Meng, S.S. Jeffrey, Oxidative stress pathways highlighted in tumor cell immortalization: association with breast cancer outcome, Oncogene 26 (2007) 6269–6279.
[65] M. Campanella, N. Parker, C.H. Tan, A.M. Hall, M.R. Duchen, IF(1): setting the pace of the F(1)F(o)-ATP synthase, Trends Biochem. Sci. (2009) 343–350.
[66] A.I. Jonckheere, M. Huigsloot, M. Lammens, J. Jansen, L.P. van den Heuvel, U. Spiekerkoetter, J.C. von Kleist-Retzow, M. Forkink, W.J.H. Koopman, R. Szklarczyk, M.A. Huynen, J.A. Fransen, J.A.M. Smeitink, R.J. Rodenburg, Restoration of complex V deficiency caused by a novel deletion in the human TMEM70 gene normalizes mitochondrial morphology, Mitochondrion 11 (2011) 954–963.
[67] C.D.L. Folmes, T.J. Nelson, A. Martinez-Fernandez, D.K. Arrell, J. Zlatkovic Lindor, P.P. Dzeja, Y. Ikeda, C. Perez-Terzic, A. Terzic, Somatic oxidative bioenergetics transitions into pluripotency-dependent glycolysis to facilitate nuclear reprogramming, Cell Metab. 14 (2011) 264–271.